Numerical Comparison between a Modern Surfboard and an Alaia Board using Computational Fluid Dynamics (CFD)

Luca Oggiano
Norwegian University of Science and Technology – SIAT (Senter for Idrettsanlegg og Teknologi), K. Hejes Vei 2b 7042, Trondheim, Norway
IFE -Institutt for Energiteknikk, Instituttveien 18a, 2007, Kjeller, Norway

Keywords: Hydrodynamics, CFD, Surfboard Design.

Abstract: Surfboard design is traditionally considered more as an art than an engineering process. However, in the past decade, the use of computers is becoming the standard in the shaping process. In the design part the use of computer-aid-design (CAD) software, has simplified the design process allowing shapers to save time and consistently modify or reproduce similar designs. At the same time, the improvement of computer-numerical-controlled (CNC) machines is slowly replacing the traditional hand shaping techniques with more controlled and reproducible manufacturing process. Another considerable advantage about having a 3D CAD model of the surfboard is that the model can be imported in Computational Fluid Dynamics (CFD) programs and its performances can be studied and evaluated highlighting details that would be otherwise impossible to identify from a field test. The present paper aims to show the potential of CFD solvers for surfboard design and its applicability by comparing a modern surfboard with a traditional ancient surfboard design (alaia). The performances of the modern surfboard are evaluated and compared with the alaia board, represented by an equivalent flat plate which is also used for validation. The commercial CFD code STAR-CCM+ is used in the present work. An Unsteady Reynolds Navier Stokes (URANS) approach is used, the volume of fluid (VOF) method is chosen as free surface discretization method and the turbulence model chosen to allow the numerical closure of the RANS equations is the k-ω-SST proposed by Menter. The model validation on an alaia board, represented as a flat plate shows good agreement with previous studies and the comparison between the surfboard and the alaia addresses the superiority of the modern surfboard design in terms of stability.

1 INTRODUCTION

Surfboards firstly appeared in the 5^{th}-6^{th} century in Hawaii and they were used monarchs and villagers alike. At that time, three types of surfboards were available: the paipo (used by children) the olo (long, thick and heavy boards that could weight up to 100kg) and the alaia. Surfing as we know it (standing up and riding curing waves) was developed and discovered thanks to the alaia boards. The alaia boards are middle sized boards, simple in shape, made in wood and finless, they can be resembled to flat plates with a rounded nose. The board paddles well enough to catch unbroken swells still allows manoeuvres and curves on the waves face and it is responsive to the surfer commands. For centuries, surfing and surfboard design was confined to Hawaii and no evolutions in the shape of the boards were made since modern times. For the first time, in 1930's balsa wood (much lighter than normal wodd) was introduced, the tail of the boards were tapered to have a more hydrodynamic design and increase manoeuvrability and fins were firstly introduced to increase stability . The main change in construction and materials didn't appear since the late 1940's, where fiberglass was introduced, allowing more complex shaping and finally driving the design to the modern surfboard design (Warshaw, 2010, Heimann, 2010). During this period of time, boards became lighter, smaller and their shape constantly evolved. However, the surfboard design and shaping is still seen as a form of art more than an engineering task.

Surfboards can be considered as 3D planing surfaces similar to planing boats, velles, and surface effect ship (SES) (Doctors, 2009). The main

Oggiano L.
Numerical Comparison between a Modern Surfboard and an Alaia Board using Computational Fluid Dynamics (CFD).
DOI: 10.5220/0006488400750082
In *Proceedings of the 5th International Congress on Sport Sciences Research and Technology Support (icSPORTS 2017)*, pages 75-82
ISBN: 978-989-758-269-1

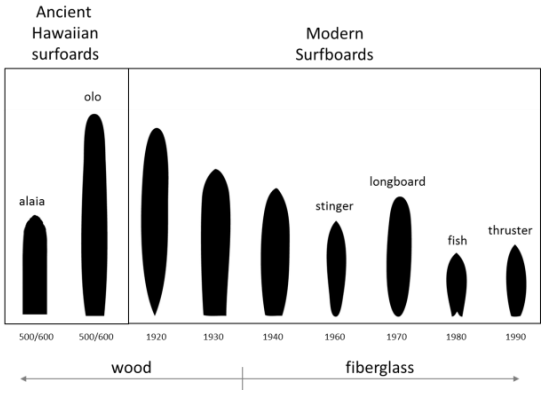

Figure 1: Evolution of surfboard design throughout the years.

difference between a planing vessel and a traditional one is that in planing vessels (and also in surfboards), the hydrodynamic lift is typically used to support a majority of the vessel displacement, whereas hydrostatic forces constitute the main contribution for displacement vessels. In order to generate the necessary amount of lift, surfboards need to reach a certain speed, however, in order to reach the high speed needed, they should first operate at a lower speed and successively accelerate in order to be able to support the surfer. The acceleration is usually obtained in two steps, in the first step the surfer paddles, accelerating in order to catch the wave and then uses the wave behaviour by pitching the board to sharply increase the speed reaching planing conditions. While the studies on surfboards are limited, the studies on planing surfaces are present in the literature and CFD proved to a useful tool to study the physics of the phenomenon. In particular Kramer (Kramer et al., 2013) studied with CFD at 2D flat plate similar in size of a alaia board.

The present paper aims to compare the planing characteristics of a modern surfboard with an alaia board with the same aspect ratio, pointing at differences and proving the efficiency of CFD as design tool for surfboards.

2 METHODS

A fully non-linear CFD approach will used throughout the paper.

2.1 Numerical Setup

The VOF (Volume of Fluid) method originally proposed by (Hirt and Nichols, 1981) included in STAR-CCM+ was used in the current simulations.

The interface capturing routine is implemented in the solver with a high-resolution compressive differencing scheme described in (Ubbink, 1997, Ferziger and Peric, 2001).

The k-ω turbulence model proposed by Menter (Menter, 1994) was used as closure model to solve a time dependent version of the Reynolds Averaged Navier Stokes. The k-ω Menter SST model was chosen due to its capabilities to capture the vortex structures developing in the wake region and its superior performances in highly separated flows (Zaïdi et al., 2010, Wilcox, 2006).

The governing equations used in the discretised model can be generally expressed as:

$$\nabla \cdot u = 0 \tag{1}$$

$$\frac{\partial u}{\partial t} + u \cdot \nabla u = -\frac{\nabla p}{\rho} + g + \nabla \cdot (\mu \nabla u) \tag{2}$$

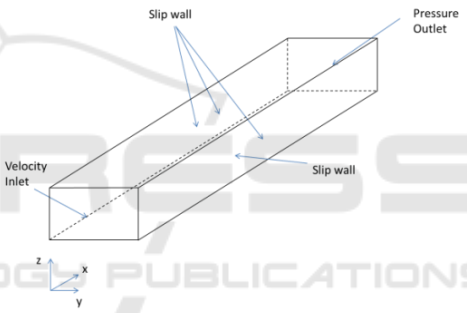

Figure 2: Numerical basin with boundary conditions applied at each boundary.

Where Eq. 1 represents the conservation of mass and Eq.2 represents the conservation of momentum. In the VOF representation, the density ρ, and the viscosity, μ, are specified in terms of the water volume fraction, α

$$\rho = \alpha \rho_{water} + \rho_{air}(1 - \alpha) \tag{3}$$

$$\mu = \alpha \mu_{water} + \mu_{air}(1 - \alpha) \tag{4}$$

When solving the equations, the water volume fraction α, once the velocity field is known, is advanced in time by the transport equation:

$$\frac{\partial u}{\partial t} + \nabla \cdot u\alpha + \nabla u_r \cdot \alpha(1 - \alpha) = 0 \tag{5}$$

Per each time step, the forces on the model are calculated by pressure integration on the pressure on the wetted surface area.

$$F(t) = \int_{wetted\ surface} p(t)d\vec{n} \quad (6)$$

The domain width is 30m, the depth is 10m and the length is 200m. The boundary conditions used in the simulation are shown in Figure 2: slip wall condition was used at the bottom, symmetry boundary conditions were used at the sides and top and a p boundary condition was used at the outlet. A relaxation area, consisting of an added damping domain with a flat bottom, 200m long and discretized with stretched cells in the x-direction was added at the end of the domain in order to reduce numerical reflection from the outlet.

2.2 Geometrical Models Used

A surfboard and a flat plate (representing the alaia) models are used in the present study, both with an initial immersed length *Li*=0.5m and oriented with an angle of attack *AoA* from the calm-water free-surface. The model is assumed to travel at a constant forward speed *U* on the water surface, which is assumed to be an incompressible fluid of density ρ_w and kinematic viscosity v_w and it represents the liquid phase of the mixture. The traveling velocity is modelled by imposing a velocity inlet boundary condition at the inlet boundary, where the velocity u_w=*U* is here prescribed to each of the boundary cells included in the liquid phase of the mixture.

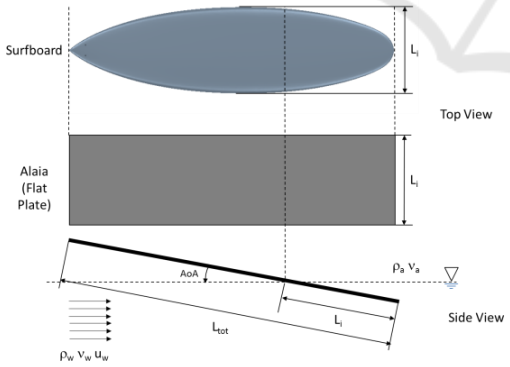

Figure 3: Side and top view of the surfboard and alaia (flat plate) models used in the simulations.

The second phase of the mixture is assumed to be air and it is modelled as an incompressible gas of density ρ_a and kinematic viscosity v_a and u_a=0.

Defining the Froude Number as

$$Fr = \frac{u_w}{\sqrt{2gL_i}} \quad (7)$$

Table 1: Physical quantities.

Item	Symbol	Value	Units
Water density	ρ_w	1000	kg/m3
Air density	ρ_a	1.19	kg/m3
Water kinematic viscosity	v_w	$1.0048 \cdot 10^{-6}$	m^2/s
Air kinematic viscosity	v_a	$1.4604 \cdot 10^{-5}$	m^2/s
Immersed length	L_i	0.5	m
Gravitational acceleration	g	9.81	m/s^2
Total length	L_{tot}	1.65	m

Where u_w is the flow velocity of the water mixture, g is the gravity and Li is the immersed length, two different flow velocities, *U*=4m/s and *U*=8m/s corresponding to *Fr*=1.28 and *Fr*=2.55 were simulated. The flow velocities are chosen in order to be representative for paddling speed (*U*=4m/s) and cruising speed (*U*=8m/s).

2.2.1 Surfboard

The surfboard model used is designed with Akkushape. The model does not include fins and it has a length of 1.65m and a width of 0.5m The tail geometry is a squash tail.

Figure 4: 3D representation of the surfboard model.

2.2.2 Alaia

The alaia model used in the simulations has the same length and width of the surfboard (length=1.65m, width= 0.5m). For simplification and in order to have comparable data available, the alaia design chosen for the simulations was a simple flat plate and its dimensions were chosen in order to have the same aspect ratio as the surfboard where:

$$Aspect\ ratio = \frac{L_{tot}}{L_i} \quad (8)$$

2.3 Grid Topology and Grid Dependence Study

A trimmed meshing technique was chosen in order to correctly model the water free surface in the numerical basin. Different levels of grid refinements were used in order correctly reproduce the perturbations to the free surface induced by the models.

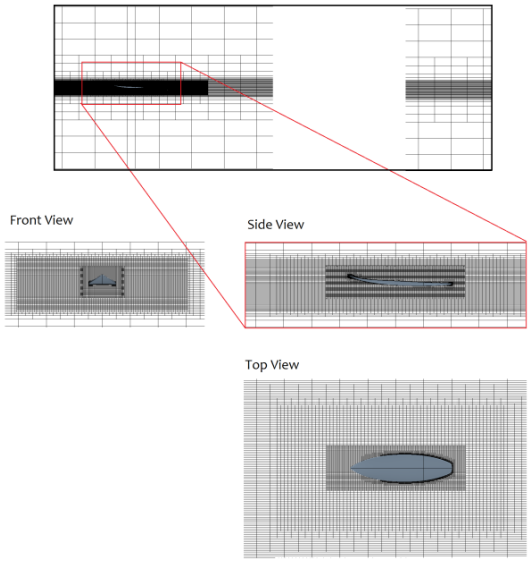

Figure 5: Mesh topology.

The surface mesh was created using 100points per curvature and a prismatic mesh consisting of 10 layers growing with a growing factor of 1.5 was created on top of the surface in order to correctly capture the boundary layer. The first cell height was chosen so that the wall y+ was kept lower than 5 on the whole surface. Defining the convective Courant number as

$$CCN = \frac{u_w \Delta t}{\Delta x} \quad (9)$$

Where u_w is the water flow velocity, Δt is the time step and Δx is the cell with in the x direction, the time step was chosen so that CCN=0.5 in the finer portion of the grid, which is the necessary condtion for the numerical stability of the VOF model.

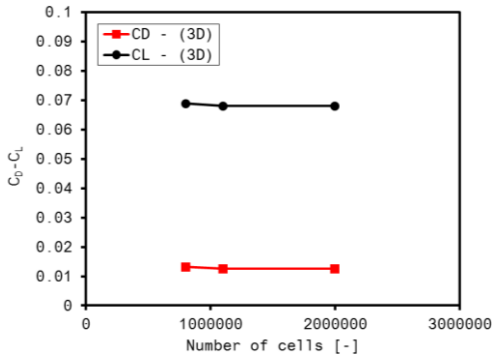

Figure 6: Grid convergence for c_L and c_D at Fr.1.1, AoA=4 deg for the surfboard.

A preliminary dependency study was carried out for AoA=4 deg and Fr=1.1 in order to ensure numerical convergence and a grid independent solution. The results are plotted in Figure 6. The plot shows a clear grid convergence with minimal differences between the middle refined grid consisting of 1.2million cells and the fine grid which consists of 2.1millions cells. The fine grid, consisting of a total number of cells of 2.1millions was used in the simulations.

2.4 Model Validation

A preliminary study on a 2D fixed flat plate was carried out in order to validate the model against previous work.

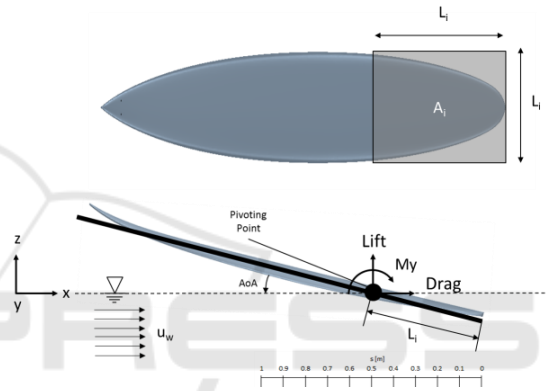

Figure 7: Surfboard parameters and coordinate system.

The problem of a two-dimensional planing flat plate studied using a nonlinear CFD solver for varying Froude number and angle of studied by Kramer (Kramer et al., 2013) was chosen for the comparative study. In Kramer's work a quasi-steady CFD approach using inviscid flow was used and potential-flow assumptions that either assume linear free-surface and body boundary conditions or ignore gravitational effects were also addressed. As a reference case, the test case with Fr=1.1 and AoA=10deg was chosen. In the present computations, a fully turbulent approach is used and both a 2D and 3D computations were carried out and compared with the previous computations carried out by Kramer.

The non dimensional coefficients for lift and drag were chosen to be relative to the direction of motion with the drag being along the x-axis and parallel to u_w and the lift in the y-axis and perpendicular to the velocity u_w. The pivoting point around which the models rotate was placed at s=0.5m.

The nondimensional coefficients for lift and drag force can be expressed as follows:

$$C_L = \frac{Lift}{\frac{1}{2}\rho_w u_w^2 A_i} \quad (10)$$

$$C_D = \frac{Drag}{\frac{1}{2}\rho_w u_w^2 A_i} \quad (11)$$

With A_i [m^2] being the submerged area and being 0.25m and 0.182m respectively for the flat plate representing the alaia and for the surfboard.
The results from the computations for both 2D and 3D cases are plotten in Figure 8.

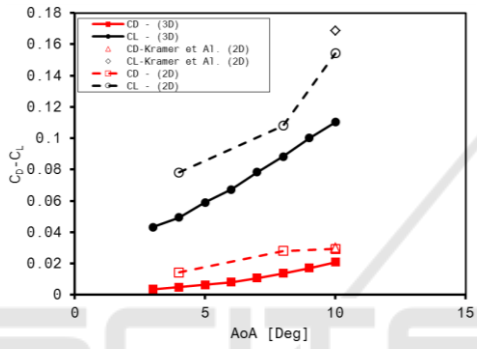

Figure 8: C_D and C_L for a 2D and 3D flat plate and comparison with previous work (Kramer et al., 2013).

A good agreement between the Kramer computations and the present one can be seen for both lift and a drag coefficient values for the 2D case. When comparing the 3D simulations with the 2D simulations, a clear decrease in drag and lift coefficient can be seen in Figure 8. This is due to the influence of the downwash from the extremity vortices resulting in reduced lift for finite aspect-ratio plates. This is a known phenomenon and it is widely addressed in the classical theory for flat plates aerodynamics (Taira and Colonius, 2009) but also in the theory for planing flat plates with different aspect ratios (Perry, 1952) and in the classical aerodynamics theory (White, 2016). The drag and lift difference due to extremity vortices can also be seen when analysing the pressure coefficient contour plots for the 2D and 3D flat plate from the simulations at AoA=10deg and Fr=1.1 (Figure 9). In the plots the pressure has been normalized with the flow velocity

$$C_P = \frac{Pressure}{\frac{1}{2}\rho_w u_w^2} \quad (12)$$

The contour plots from the 2D simulations show that the stagnation point is located at 0.85m from the trailing edge, which is in line with previous simulations while for the 3D simulations the stagnation pint is located further back in the plate at 0.7m from the trailing edge. While in the 2D simulations the iso-pressure lines are almost parallel, in the 3D simulations, a pressure drop near the sides is present. The overall lower pressure experienced by the 3D plate when compared with the 2D plate, results leads to a lower drag force but in particular a lower lift force.

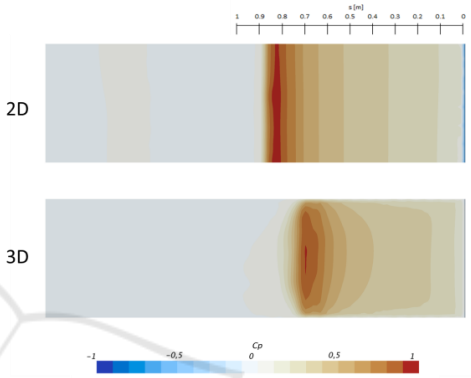

Figure 9: Iso-pressure coefficient contours on the 2D and 3D flat plate.

In Figure 10 the iso-surface representing the free water surface is shown. Here, the flow detaching from the flat plate sides that leads to a lower overall drag on the 3D flat plate is clearly visible.

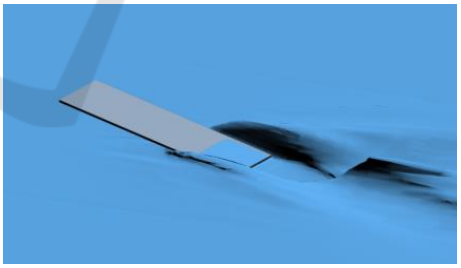

Figure 10: Free surface snapscho of the flow behind a 3D flat plate for AoA=10 and Fr=1.1.

3 RESULTS AND DISCUSSION

In the present section, the results from the simulations are evaluated and the key performances of the surfboard and the alaia board are compared.

From Figure 11 it is clearly visible the alaia has a larger drag than the surfboard. This is due to a number of factors but two main design differences

causing this behaviour can be addressed. The bottom of the boards is different with the surfboard having a curved bottom surface to deliberately reduce the drag and increase the speed. The tail shape between the two boards is also different, with the surfboard having a tapered shape (introduced in late 1920's) to allow for better performances and in particular to reduce the drag generated by the extremity vortices detachment. It is also clearly visible that the surfboard's c_D is stable with increasing speeds while a steep decrease in c_D happens in in the alaia. This leads to the need of continuous and more prominent adjustments from the rider in order to compensate for the difference in drag generated by the board and allow the surfer a smooth ride.

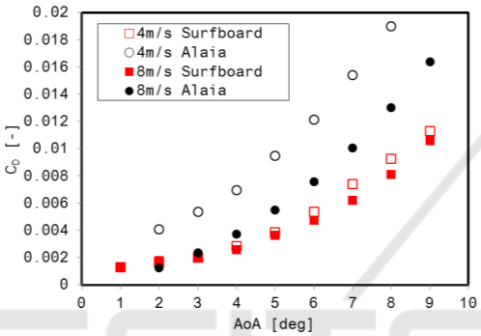

Figure 11: Drag coefficient c_D versus Angle of Attack *AoA* for alaia and surfboard at 4m/s and 8m/s. Surfboard in red (■) and alaia in black (●).

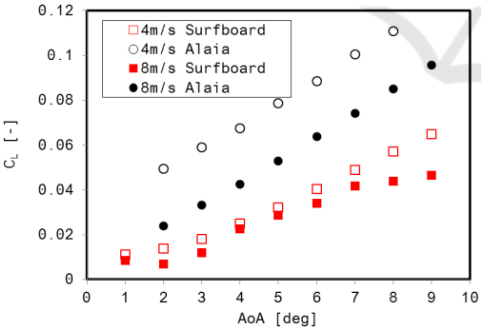

Figure 12: Lift coefficient c_L versus Angle of Attack *AoA* for alaia and surfboard at 4m/s and 8m/s. Surfboard in red (■) and alaia in black (●).

The alaia also generates a greater lift than the surfboard due to the topology of its bottom deck when compared with the surfboard.

A flatter bottom like the one found in the alaia leads to a larger wetted area and thus larger forces both in the horizontal and vertical direction. This also explains the fact that alaias require considerable smaller volumes to be able to plane.

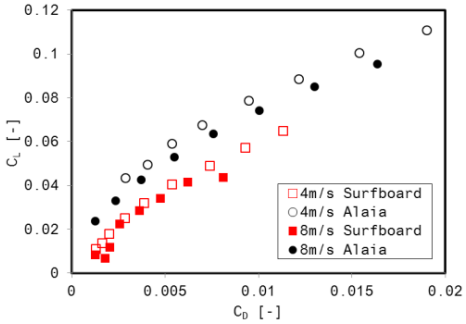

Figure 13: Lift coefficient c_L versus drag coefficient c_D for alaia and surfboard at 4m/s and 8m/s. Surfboard in red (■) and alaia in black (●).

Similar conclusions can be drawn when plotting the polar curve (c_L vs. c_D) for both surfboard and alaia with the latter one generating higher lift for the same levels of drag when compared with the surfboard.

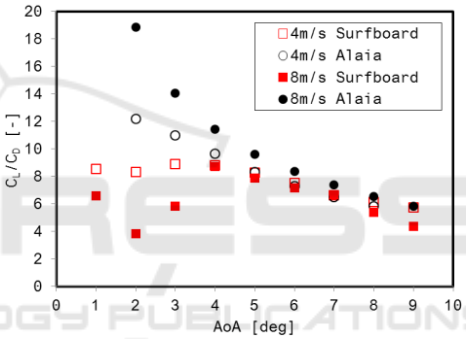

Figure 14: Efficiency (c_L/c_D) versus Angle of Attack *AoA* for alaia and surfboard at 4m/s and 8m/s. Surfboard in red (■) and alaia in black (●).

When plotting the efficiency (c_L/c_D) against the angle of attack (Figure 14), a different behaviour between the alaia and the surfboard can be noticed, with the latter having a lower efficiency at low angles of attack but a more constant efficiency than the former. The higher lift generated by the alaia at low angles of attack is due to the different pressure distribution that the alaia experiences when compared with the surfboard in the tail region (Figure 15). This high pressure in the tail region generates a negative moment that the surfer will have compensate by moving his weight on his back foot and changing the *AoA* in order to keep the board stable. In general then the high efficiency at low angles of attack for the alaia is generated by an unstable pressure distribution and requires continuous adjustments from the surfer in order to compensate the lift generated in the tail area of the board.

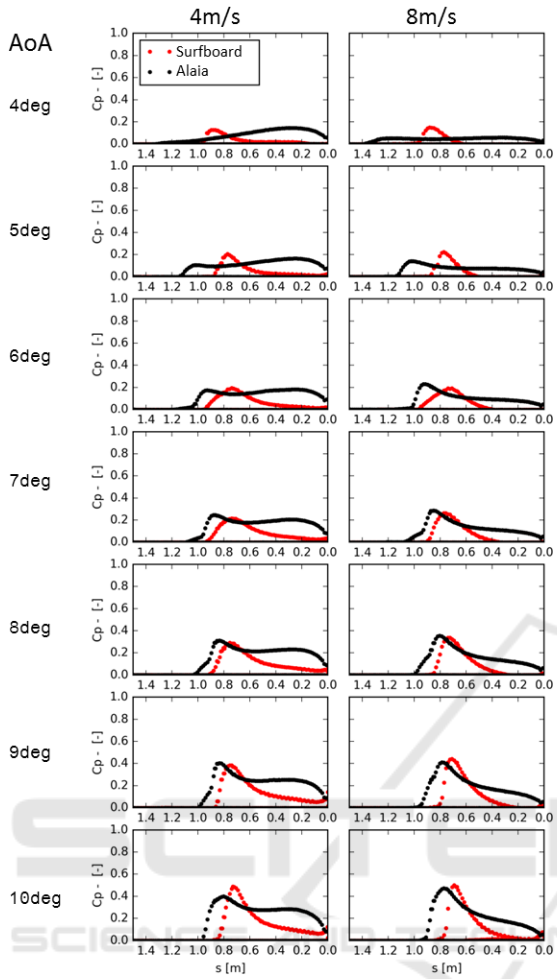

Figure 15: Pressure coefficient plots at the middle section of the models: surfboard in red (●) and alaia in black (●).

Figure 15 shows how the pressure distribution varies at different angles of attack on the alaia and on the surfboard. Due to the increased curvature of the bottom, the peak in pressure distribution on the surfboard is constantly placed at ca. *s*=0.7m, close to the front foot placement thus allowing the surfer to always feel the same behaviour of the board under his feet. It is also important to notice that the pressure distribution at 4m/s and 8m/s is similar and thus almost speed independent. The pressure distribution of the alaia, on the other hand, varies both with *AoA* and with speed, forcing the surfer to apply continuous corrections in order to keep the board balanced. It is also clearly noticeable that the alaia has a larger wetted area, which directly reflects on higher forces and higher pressure on the bottom deck, resulting then in higher lift and drag.

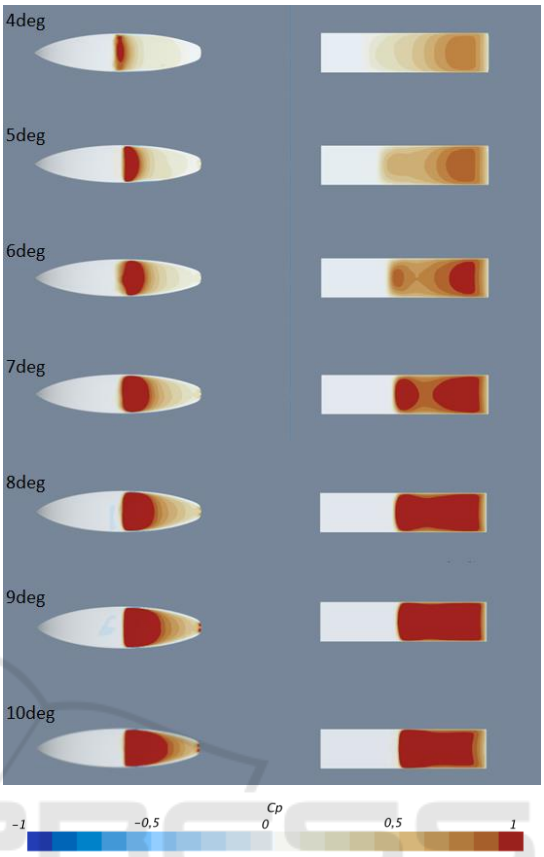

Figure 16: Pressure distribution on the surfboard (left) and alaia (right) at *U*=8m/s.

When analysing the 3D pressure contour plots on the surfboard and on the alaia for 8m/s plotted in Figure 16, the same behaviour noticeable in the pressure distributions plots in Figure 15 can be highlighted, with the surfboard keeping the maximum pressure close to where the front foot is placed and thus allowing a smoother ride to the surfer without constant corrections. When comparing the wakes generated by the surfboard and the alaia (Figure 17) the wake generated by the surfboard results clearly smaller than the wake generated by the alaia, directly leading to a lower drag. This is again due to the different tail shape and bottom shape between the the two boards with the alaia needing to move more water in order to be able to travel at the same speed of the surfboard and thus generating a wider and deeper wake.

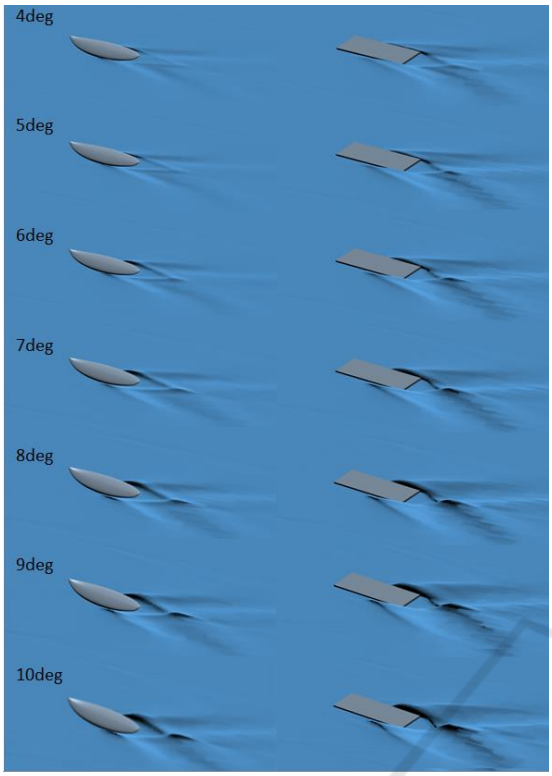

Figure 17: Free and wake development on the surfboard (left) and alaia (right) at U=8m/s.

4 CONCLUSIONS

CFD simulations proved to be a useful tool and to evaluate and compare the performances of a surfboard against an alaia with the same aspect ratio. The fixed model approach has is however only useful if used for qualitative comparisons or design since it does not take into consideration buoyancy and trimming. Overall the performances of the surfboard showed a clear superiority in longitudinal stability when compared with the alaia while the alaia, mostly due to the flat bottom inducing a larger wetted area resulted to have higher drag but also higher lift, however, the strong dependency of the generated lift to speed and *AoA* and the placement of the pressure on the bottom deck, lead to continuous adjustments needed in order to stabilize the board.

ACKNOWLEDGMENTS

The author would like to thank Max Leinenbach for providing the surfboard CAD model.

REFERENCES

Ferziger, J. H. & Peric, M. 2001. *Computational Methods for Fluid Dynamics*, Springer - London.

Heimann, J. 2010. *Surfing*.

Hirt, C. W. & Nichols, B. D. 1981. Volume of Fluid (Vof) Method for the Dynamics of Free Boundaries. *Journal of Computational Physics,* 39**,** 201-225.

Kramer, M. R., Maki, M. J. & Young, Y. L. 2013. Numerical Prediction of the Flow Past A 2-D Planing Plate At Low Froude Number. *Ocean Engineering,* 70**,** 110–117.

Menter, F. R. 1994. Two-Equation Eddy-Viscosity Turbulence Models for Engineering Applications. *Aiaa Journal,* 32**,** 1598–1605.

Perry, B. 1952. The Effect of Aspect Ratio on the Lift of Flat Planing Surfaces. Pasadena: Hydrodynamics Laboratory California Insitute of Technology.

Taira, K. & Colonius, T. 2009. Three-Dimensional Flows Around Low-Aspect-Ratio Flat-Plate Wings At Low Reynolds Numbers. *J. Fluid Mech.,* 623**,** 187–207.

Ubbink, O. 1997. *Numerical Prediction of Two Fluid Systems With Sharp Interfaces*, Phd Thesis Submitted To The University of London and Diploma of Imperial College.

Warshaw, M. 2010. *The History of Surfing*.

White, F. M. 2016. *Fluid Mechanics (8th Eidition)*, Mcgraw-Hill Book Co, New York, USA.

Wilcox, D. C. 2006. *Turbulence Modelling for Cfd,* La Canada, California, USA.

Zaïdi, H., Fohanno, S., Taïar, R. & Polidori, G. 2010. Turbulence Model Choice For The Calculation of Drag Forces When Using The Cfd Method. *Journal of Biomechanics,* 10**,** 405-11.